 CMES, vol.2, no.3, pp.307-318, 2001

Meshless Regular Hybrid Boundary Node Method

Jianming Zhang, Zhenhan Yao[1]

Abstract: The Meshless Local Boundary Integral Equation (MLBIE) method is a truly meshless one as it does not need a 'finite element or boundary element mesh', either for variable interpolation or for 'energy' integration. The Boundary Node Method (BNM) further reduces the dimensionality of the problem by one, i.e. it only requires nodes constructed on the surface. However, the BNM is not truly meshless, as a background mesh is needed for boundary integration; and the MLBIE does not have the advantage of reduced dimensionality as the BNM. A new Regular Hybrid Boundary Node method based on a modified functional and the Moving Least Squares (MLS) approximation, and combining the advantages of both the MLBIE and the BNM, is presented in this paper.

The Regular Hybrid Boundary Node Method is formulated in terms of the domain and boundary variables. The domain variables are interpolated by classical fundamental solutions with the source points located outside the domain; and the boundary variables are interpolated by Moving Least-Squares (MLS) approximation. The main idea is to retain the dimensionality advantages of the BNM, and localize the integration domain to a regular sub-domain, as in the MLBIE, such that no mesh is needed for integration. All integrals can be easily evaluated over regular shaped domains (in general, semi-circle in the 2-D problem) and their boundaries.

Numerical examples for the solution of 2-D Laplace equation show that the high convergence rates with mesh refinement and the high accuracy with a small node number are achievable. The treatment of singularities and further integrations required for the computation of the unknown domain variables, as in the conventional BEM and BNM, can be avoided.

[1] Department of Engineering Mechanics,
Tsinghua University, Beijing, 100084
China
Telephone: +8610-62772913
E-mail: demyzh@tsinghua.edu.cn

1 Introduction

Although the FEM and BEM have made great achievements in solving practical engineering problems, the interest of pursuing new methods has never decreased through time, as the mesh-based methods (e.g. FEM and BEM) have much difficulty in solving problems involving changing domains such as large deformation or crack propagation; and the task of mesh generation of a 3-D object with complicated geometry is often arduous, time-consuming and computationally expensive, in spite of significant progress has been made in 3-D meshing algorithms. In recent years, novel computational algorithms, referred to as 'meshless' methods, have been proposed, that largely circumvent the problems associated with meshing.

The idea of meshless methods was initially introduced by Lucy as the Smooth Particle Hydrodynamics (SPH) method for modeling astrophysical phenomena (1977), although the meshless methods first gained popularity after the publication of the diffuse element method (Nayroles et al., 1992) and the element free Galerkin method (Belytschko et al., 1994). The element free Galerkin (EFG) method uses a global symmetric weak form and the shape functions from the moving least-squires approximation. Although no mesh is required in the EFG method for the variable interpolation, background cells are inevitable for the 'energy' integration.

Recently, two meshless methods, the Meshless Local Boundary Integral Equation (MLBIE) method (Zhu et al., 1998; Kim and Atluri, 2000; Lin and Atluri, 2000) and the Meshless Local Petrov-Galerkin (MLPG) approach (Atluri et al., 1998) have been developed. Both methods use local weak forms over a local sub-domain and shape functions from the MLS approximation, and lead to truly meshless ones, as no 'finite element or boundary element mesh' is required either for the variable interpolation, or for the 'energy' integration. All integrals can be easily evaluated over regularly shaped domains (for example, circles in 2-D problems and spheres

in 3-D problems) and their boundaries.

Previously, Mukherjee et al. (1997) proposed a meshless method, which they call the Boundary Node Method (BNM). They combined the MLS interpolants with Boundary Integral Equations (BIE) in order to retain both the meshless attribute of the former and the dimensionality advantage of the latter. This method only requires a nodal data structure on the bounding surface of a body whose dimension is one less than that of the domain itself; but this method is not a truly meshless one, as an underlying cell structure is again used for numerical integration.

A question arises here– is there possibly a method of solving boundary value problems, that only requires nodes constructed on the surface of a domain and requires no cells either for interpolation of the solution variables or for the numerical integration? This method will simplify the input data structure greatly, as it has the dimensionality advantage of the BIE and only requires scattered nodes on the boundary, compared with the MLBIE and MLPG; and it is a truly meshless method, which does not use any mesh either for interpolation or for integration, compared with the BNM.

The answer is positive. The new method is called Hybrid Boundary Node Method (Hybrid BNM)(Zhang et al.), which combines the MLS interpolation scheme with the hybrid displacement variational formulation. However, the Hybrid BNM has a drawback of serious "boundary layer effect", i.e. the accuracy of results in the vicinity of the boundary is very sensitive to the proximity of the interior points to the boundary. A new Regular Hybrid Boundary Node method is proposed in this paper. In the new method, the source points of the fundamental solutions are located outside the domain other than at the boundary nodes as in the Hybrid BNM or other hybrid boundary element models. Compared with the Hybrid BNM, the present method does not involve any singular integration and the results are no more sensitive to the proximity of the interior points to the boundary, very high accuracy can be achieved with a small number of boundary nodes.

The hybrid boundary element method was first proposed by Schnack (1987), in which he stressed using the boundary element method to generate a hybrid stress finite element model, giving rapid convergence of the results and accurate solution for stress concentration problems. Dumont (1987) has presented a hybrid stress boundary element formulation based on Hellinger-Reissner principle with stresses in the domain and displacements on the boundary as independent functions. DeFigueredo and Brebbia (1989) have introduced a hybrid displacement variational formulation of BEM, which is based on a modified functional using three independent variables, i.e. displacements and tractions on the boundary and displacements inside the domain. This approach uses the classical fundamental solution to interpolate the displacements in the domain and thus allowing for the transfer of the domain integrals to the boundary. The resulting system of equations is written in terms of boundary displacements only, and has the advantage of being symmetrical, which is easy to couple with the FEM. In the present paper, the objective is not to obtain the symmetrical system of equations in terms of boundary displacements, we just use the hybrid displacement variational formulation and the interpolation scheme of variables inside the domain. The variables on the boundary are interpolated by MLS scheme and a truly meshless RHBNM is achieved.

The following discussion begins with the brief description of the MLS approximation in Section 2. Taking Laplace equation as an example, the formulation of RHBNM is developed in Section 3. Numerical examples for 2-D potential problems are given in Section 4. The paper ends with conclusions and discussions in Section 5.

2 The MLS approximation scheme for the 2-D Regular Hybrid Boundary Node method

This section gives a brief summary of the MLS approximation, of which excellent illustrations can be seen in papers (Belytchko et al. 1996; Lancaster et al. 1981).

The discussion below addresses the solution u of a scalar problem (Laplace equation) in 2-D. In the view of the fact that this MLS interpolation scheme will be coupled later with 2-D hybrid 'displacement' variational formulation which uses three independent variables, of which the $\tilde{u}$ and $\tilde{q}$ are defined as the potential and normal flux on the 1-D bounding surface Γ of a 2-D body Ω, and will be interpolated by MLS scheme.

The difference of MLS interpolation between the present approach and the BNM is that in the present approach, MLS interpolation is independently performed on piecewise smooth segments $\Gamma_i, i = 1, 2, \cdots, n$ which consist the boundary naturally other than on the whole bound-

ary Γ. To approximate the functions $\tilde{u}$ and $\tilde{q}$ on each Γ_i over which a number of randomly located nodes $\{s_I\}, I = 1,2,\cdots,N$, the MLS interpolants for $\tilde{u}$ and $\tilde{q}$ are defined as

$$\tilde{u}(s) = \sum_{j=1}^{m} p_j(s)a_j(s) = p^T(s)a(s) \tag{1}$$

$$\tilde{q}(s) = \sum_{j=1}^{m} p_j(s)b_j(s) = p^T(s)b(s) \tag{2}$$

where s is a curvilinear co-ordinate (here the arc length) on Γ_i, $p_1 = 1$ and $p_j(s), j = 2,\cdots,m$ are monomials in s. The monomials $p_j(s)$ provide the intrinsic polynomial bases for $\tilde{u}$ and $\tilde{q}$. In the numerical implementation presented later in this paper, a quadratic background basis is used, i.e.

$$p^T(s) = [1, s, s^2], \qquad m = 3 \tag{3}$$

The coefficient vector $a(s)$ and $b(s)$ is determined by minimizing a weighted discrete L_2 norm, defined as

$$J_1(s) = \sum_{I=1}^{N} w_I(s)\left[p^T(s_I)a(s) - \hat{u}_I\right]^2 \tag{4}$$

$$J_2(s) = \sum_{I=1}^{N} w_I(s)\left[p^T(s_I)b(s) - \hat{q}_I\right]^2 \tag{5}$$

where points s_I are boundary nodes on Γ_i, s is the co-ordinate of an evaluation point E on Γ_i, N is the number of boundary nodes in the neighborhood of E for which the weight functions $w(s - s_I) > 0$. It should be noted here that $\hat{u}_I$ and $\hat{q}_I, I = 1,2,\cdots,N$ are the fictitious nodal values other than the nodal values of the unknown $\tilde{u}_I$ and $\tilde{q}_I$ in general. This distinction between $\hat{u}_I$ and $\tilde{u}_I$ (or $\hat{q}_I$ and $\tilde{q}_I$) is very important in the view of the fact that MLS interpolants lack the delta function property.

Solving for $a(s)$ and $b(s)$ by minimizing J_1 and J_2 in equation (4) and (5), and substituting them into equation (1) and (2) gives a relation which may be written as the form of an interpolation function similar to that used in the FEM, as

$$\tilde{u}(s) = \sum_{I=1}^{N} \Phi_I(s)\hat{u}_I \tag{6}$$

$$\tilde{q}(s) = \sum_{I=1}^{N} \Phi_I(s)\hat{q}_I \tag{7}$$

where

$$\Phi_I(s) = \sum_{j=1}^{m} p_j(s)\left[A^{-1}(s)B(s)\right]_{jI} \tag{8}$$

with the matrices $A(s)$ and $B(s)$ being defined by

$$A(s) = \sum_{I=1}^{N} w_I(s)p(s_I)p^T(s_I) \tag{9}$$

$$B(s) = [w_1(s)p(s_1), w_2(s)p(s_2), \cdots, w_N(s)p(s_N)] \tag{10}$$

The MLS approximation is well defined only when the matrix A in equation (9) is non-singular.

The function $\Phi_I(s)$is usually called the shape function of the MLS approximation corresponding to nodal point s_I. From equation (8) and (10), it may be seen that $\Phi_I(s) = 0$ when $w_I(s) = 0$. The fact that $\Phi_I(s)$ vanishes for s not in the support of nodal point s_I preserves the local character of the MLS approximation.

Several kinds of weight function can be seen in the literatures, the choice of weight functions and the consequences of a choice in the EFG method are discussed in some detail elsewhere (Belytchko et al. 1996). Gaussian weight function corresponding to node s_I may be written as

$$w_I(s) = \begin{cases} \frac{\exp[-(d_I/c_I)^2] - \exp[-(\hat{d}_I/c_I)^2]}{1 - \exp[-(\hat{d}_I/c_I)^2]}, & 0 \le d_I \le \hat{d}_I \\ 0, & d_I \ge \hat{d}_I \end{cases} \tag{11}$$

where $d_I = |s - s_I|$, the absolute value of the distance between an evaluation point and a node, measured along Γ_i, c_I is a constant controlling the shape of the weight

function, and $\hat{d}_I$ is the size of the support for the weight function w_I and determines the support of node s_I. The $\hat{d}_I$ should be chosen such that $\hat{d}_I$ should be large enough to have sufficient number of nodes covered in the domain of definition of every sample point $(N \geq m)$ to ensure the regularity of A.

3 Development of the Regular Hybrid Boundary Node method

In this section, the development of the Regular Hybrid Boundary Node Method is illustrated by the following potential problem:

$$\begin{aligned} &u_{,ii} = 0, \quad \forall x \in \Omega \\ &u = \overline{u}, \quad \forall x \in \Gamma_u \\ &u_{,i} n_i \equiv q = \overline{q}, \quad \forall x \in \Gamma_q \end{aligned} \tag{12}$$

where the domain Ω is enclosed by $\Gamma = \Gamma_u + \Gamma_q$; $\overline{u}$ and $\overline{q}$ are the prescribed potential and normal flux respectively, on the essential boundary Γ_u and on the flux boundary Γ_q; and n is the outward normal direction to the boundary Γ, with n_i components.

The Regular Hybrid Boundary Node method proposed in this paper is based on a modified variational principle. The functions assumed to be independent are:

– potential field in the domain, u;

– boundary potential field, $\tilde{u}$;

– boundary normal flux, $\tilde{q}$.

The corresponding variational functional Π_{AB} is defined as follows:

$$\Pi_{AB} = \int_\Omega \frac{1}{2} u_{,i} u_{,i} d\Omega - \int_\Gamma \tilde{q}(u - \tilde{u}) d\Gamma - \int_{\Gamma_q} \overline{q} \tilde{u} d\Gamma \tag{13}$$

where, the boundary potential $\tilde{u}$satisfies the essential boundary condition, i.e.,$\tilde{u}$=$\overline{u}$ on Γ_u.

By carrying out the variations it can be shown that:

$$\begin{aligned} \delta\Pi_{AB} = &\int_\Gamma (q - \tilde{q}) \delta u d\Gamma - \int_\Omega u_{,ii} \delta u d\Omega \\ &+ \int_{\Gamma_q} (\tilde{q} - \overline{q}) \delta\tilde{u} d\Gamma - \int_\Gamma (u - \tilde{u}) \delta\tilde{q} d\Gamma \end{aligned} \tag{14}$$

The vanishing of $\delta\Pi_{AB}$ for arbitrary variations δuin Ω, $\delta\tilde{u}$ and $\delta\tilde{q}$ on Γ, with $\delta\tilde{u} = 0$ on Γ_u, gives the following Euler equations:

$$\begin{aligned} &u_{,ii} = 0, \quad in \quad \Omega \\ &u - \tilde{u} = 0, \quad on \quad \Gamma \\ &q - \tilde{q} = 0, \quad on \quad \Gamma \\ &\tilde{q} - \overline{q} = 0, \quad on \quad \Gamma_q \end{aligned} \tag{15}$$

Consequently the solution of the problem is now given in terms of the functions u, $\tilde{u}$ and $\tilde{q}$, which makes $\delta\Pi_{AB}$ stationary.

With the vanishing of $\delta\Pi_{AB}$, one also has the following equivalent integral equations:

$$\int_\Gamma (q - \tilde{q}) \delta u d\Gamma - \int_\Omega u_{,ii} \delta u d\Omega = 0 \tag{16}$$

$$\int_\Gamma (u - \tilde{u}) \delta\tilde{q} d\Gamma = 0 \tag{17}$$

$$\int_{\Gamma_q} (\tilde{q} - \overline{q}) \delta\tilde{u} d\Gamma = 0 \tag{18}$$

If we impose the flux boundary condition, $\tilde{q} = \overline{q}$, just the same way as the essential boundary condition after the matrices have been computed, the equation (18) will be satisfied. So it can be ignored temporarily in the following development.

It can be seen that the equation (16) and (17) holds in any sub-domain, for example, in a sub-domain Ω_s and its boundary Γ_s and L_s (See Figure 1). The following developing idea is from Zhu (1999). Actually, to follow the developing process in Zhu (1999), we use the following weak forms on a sub-domain Ω_s and its boundary Γ_s and L_s to replace equation (16) and (17):

$$\int_{\Gamma_s + L_s} (q - \tilde{q}) v d\Gamma - \int_{\Omega_s} u_{,ii} v d\Omega = 0 \tag{19}$$

$$\int_{\Gamma_s + L_s} (u - \tilde{u}) v d\Gamma = 0 \tag{20}$$

where v is a test function. It should be noted further that the above equations hold irrespective of the size and the shape of Ω_s and its boundary $\partial\Omega_s$. This is an important observation, which forms the basis for the following development. We now deliberately choose a simple

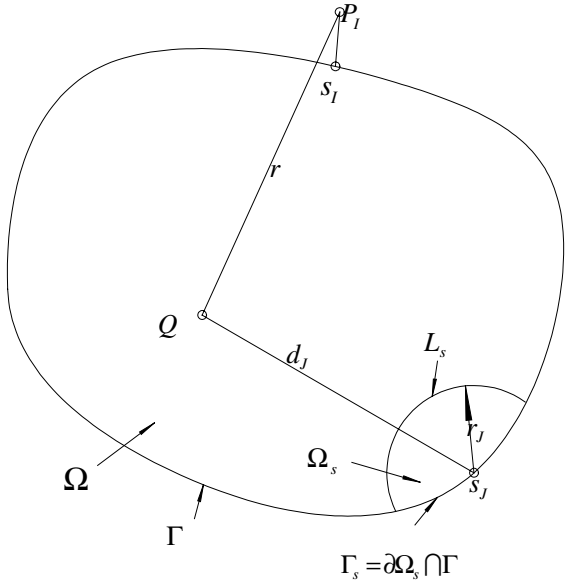

Figure 1 : The local domain centered at a node s_J and the source point of fundemental solution corresponding to a node s_I.

regular shape for Ω_s. The most regular shape of a sub-domain should be an n-dimensional sphere for a boundary value problem defined on an n-dimensional space. In the present paper, the sub-domain Ω_s is chosen as the intersection of the domain Ω and a circle centered at a boundary node s_J (See Fig. 1).

In equation (19) and (20), $\tilde{u}$ and $\tilde{q}$ on Γ_s are expressed by equation (6) and (7), but $\tilde{u}$ and $\tilde{q}$ on L_s has not been defined yet. To solve this problem, we deliberately select v such that all integrals over L_s vanish. This can be easily accomplished by using the weight function in the MLS approximation as v, with the radius $\hat{d}_I$ of the support of the weight function being replaced by the radius r_J of the sub-domain Ω_s, i.e.

$$v_J(Q) = \begin{cases} \frac{\exp[-(d_J/c_J)^2]-\exp[-(r_J/c_J)^2]}{1-\exp[-(r_J/c_J)^2]}, & 0 \le d_J \le r_J \\ 0, & d_J \ge r_J \end{cases} \tag{21}$$

where d_J is the distance between a point Q, in the domain Ω, and the nodal point s_J. Therefore, v vanishes on L_s.

The u and q inside Ω and on Γ are defined as

$$u = \sum_{I=1}^{NN} U_I x_I \tag{22}$$

$$q = \sum_{I=1}^{NN} \frac{\partial U_I}{\partial n} x_I \tag{23}$$

where U_I is the fundamental solution with the source at a point P_I, which locates at the outside of the domain and is corresponding to a node s_I; x_I are unknown parameters; NN is the total number of boundary nodes.

For 2-D potential problem, the fundamental solution is

$$U_I = \frac{1}{2\pi} \ln r(Q, P_I) \tag{24}$$

where Q and P_I are the field point and the source point respectively. And P_I is determined by following equations

$$\begin{aligned} x(P_I) &= x(S_I) + h \times n_x \times SF \\ y(P_I) &= y(S_I) + h \times n_y \times SF \end{aligned} \tag{25}$$

where x and y are coordinates; h is the mesh size; n_x and n_y is the components of the outward normal direction to the boundary at node P_I; and SF is a scale factor. As can be imagined, the scale factor, SF, plays an important role in the performance of the present method. Too small value for SF will lead to nearly-singular integrals and thus inaccurate results; On the contrary, too large one will lead to an ill-posed system of algebraic equations as well. From our computations, the proper range for SF is between 3.0 and 6.0.

As u is expressed by equation (22), the last integral in the left hand in equation (19) vanishes. By substituting equation (6), (7), (21), (22) and (23) into equation (19) and (20), and omitting the vanished terms, one has:

$$\begin{aligned} \sum_{I=1}^{n} \int_{\Gamma_s} \frac{\partial U_I}{\partial n} v_J(Q) x_I d\Gamma &= \sum_{I=1}^{n} \int_{\Gamma_s} \Phi_I(s) v_J(Q) \hat{q}_I d\Gamma \\ \sum_{I=1}^{n} \int_{\Gamma_s} U_I v_J(Q) x_I d\Gamma &= \sum_{I=1}^{n} \int_{\Gamma_s} \Phi_I(s) v_J(Q) \hat{u}_I d\Gamma \end{aligned} \tag{26}$$

Using the above equations for all nodes, one can obtain the following system of equations:

$$Ux = H\hat{q} \tag{27}$$

$$Vx = H\hat{u} \tag{28}$$

where

$$U_{IJ} = \int_{\Gamma_s^J} \frac{\partial U_I}{\partial n} v_J(Q) d\Gamma$$

$$V_{IJ} = \int_{\Gamma_s^J} U_I v_J(Q) d\Gamma$$

$$H_{IJ} = \int_{\Gamma_s^J} \Phi_I(s) v_J(Q) d\Gamma$$

$$x^T = [x_1, x_2, \cdots, x_n]$$
$$\hat{q}^T = [\hat{q}_1, \hat{q}_2, \cdots, \hat{q}_n]$$
$$\hat{u}^T = [\hat{u}_1, \hat{u}_2, \cdots, \hat{u}_n]$$

The evaluation of the matrices $U$and V is much more simple in this approach than in BEM and BNM. No integrations of singular functions are involved, as the source points of fundamental solutions are determined by equations (25).

For a well-posed problem, either u or q are known at each node on the boundary. However, transformations between $\hat{u}_I$ and $\tilde{u}_I$, $\hat{q}_I$ and $\tilde{q}_I$ must be performed due to that the MLS interpolants lack the delta function property of the usual BEM shape functions (Atluri et al. 1999). For u prescribed edges, $\hat{u}_I$ can be obtained by

$$\hat{u}_I = \sum_{J=1}^{N} R_{IJ}\tilde{u}_J = \sum_{J=1}^{N} R_{IJ}\overline{u}_J \tag{29}$$

and for q prescribed edges, $\hat{q}_I$ can be obtained by

$$\hat{q}_I = \sum_{J=1}^{N} R_{IJ}\tilde{q}_J = \sum_{J=1}^{N} R_{IJ}\overline{q}_J \tag{30}$$

where $R_{IJ} = [\Phi_J(s_I)]^{-1}$. Therefore, by rearranging the governing equations (27) and (28), one obtains the final system in term of x only, and the unknown vector x is obtained by solving the final equations system.

Potential u and flux q at any point inside domain Ω or on boundary Γ are evaluated by equation (22) and (23) without further integrations. Since u and q on boundary Γ can be evaluated the same way as that inside domain, the unknowns $\hat{q}$ and $\hat{u}$ need not to be obtained and thus the evaluation of inverse matrix V^{-1} is avoided contrary to that in the Hybrid BNM (Zhang et al.).

From the above development, one can see that the present method is a truly meshless one, as absolutely no boundary elements are needed, either for interpolation purpose or for integration purpose. No further integration is needed in the 'post-processing' step.

4 Illustrative numerical results

A few illustrative numerical results from the RHBNM, together with comparisons with exact solutions, follow. In all cases, the Laplace equation $\nabla^2 u = 0$ is solved, together with appropriate prescribed boundary conditions. For the purpose of error estimation and convergence studies, a 'global' L_2 norm error, normalized by $|u|_{\max}$ is defined as

$$e = \frac{1}{|u|_{\max}} \sqrt{\frac{1}{N}\sum_{i=1}^{N} (u_i^{(e)} - u_i^{(n)})^2} \tag{31}$$

where $|u|_{\max}$ is the maximum value of u over N sample points, the superscripts (e) and (n) refer to the exact and numerical solutions, respectively.

In all examples, the size of support for weight function, $\hat{d}_I$ in equation (11), is taken to be $9.5h$, with h being the mesh size, and the parameter c_I is taken to be such that $\hat{d}_I / c_I$ is constant and equal to 4.0. The size of the local domain (radius r_J) for each node is chosen as $1.0h$ in all computations and the parameter c_J in equation (21) is taken to be such that r_J / c_J is constant and equal to 4.0. In all integrations, 5 Gauss points are used on each section of two half-parts of Γ_s.

4.1 Dirichlet problem on a circle

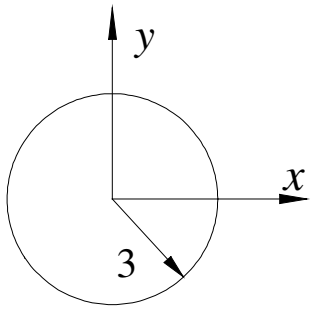

Example 1 Dirichlet problem on a circle

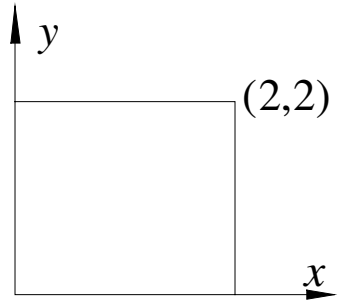

Example 2 Dirichlet, Neumann and mixed problems on a square

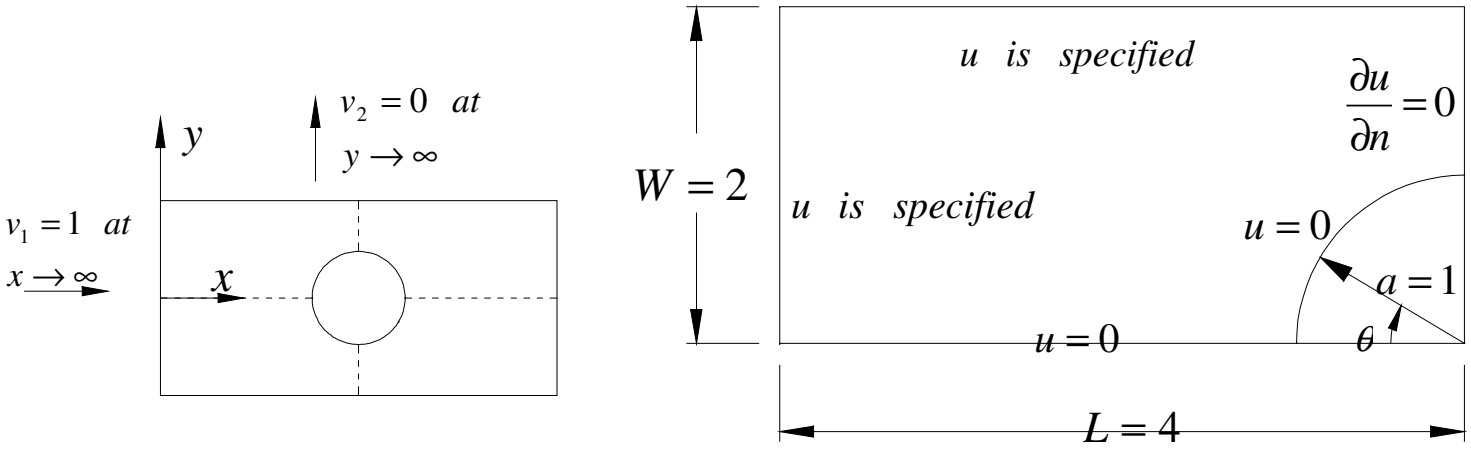

Example 3 Flow around a cylinder in an infinite field and the model with boundary conditions

Figure 2 : Geometry and boundary conditions for the examples

The example solved here is the Laplace equation on a circle of radius 3 unit, centered at the origin (See Fig. 2). The exact solution is

$$u = x \tag{32}$$

A Dirichlet problem is solved, for which the essential boundary condition is imposed on the whole circle. To study the convergence of the present method, three regular meshes of 10, 20 and 40 nodes have been used. Numerical results of u and q (with normal vector (1,0)) along the radius (form (0,0) to (3,0)) from the RHBNM with $SF = 5.0$ and from the Hybrid BNM, together with the exact solution, are shown in Fig. 3.

Results for potentials are in all case accurate. The internal fluxes from the Hybrid BNM, however, show considerable error for points close to the boundary when a small number of nodes are used. This is to be expected as they are calculated as a superposition of fundamental solutions of higher order of singularity than the ones used for the potentials (equations (22) and (23)) when the source points of fundamental solution locate exactly at the boundary nodes. The results improved considerably when the RHBNM is used. In the RHBNM, it is very appealing that very high accuracy can be achieved with a small number of nodes, and the results is no more sensitive to the proximity of the interior points to the boundary whereas in the Hybrid BNM or other hybrid boundary element methods.

4.2 *Dirichlet, Neumann and mixed problem on a squire*

The case of Laplace equation on a 2×2 domain is presented as the second example, see Fig. 2. The exact solution is a cubic polynomial

$$u = -x^3 - y^3 + 3x^2y + 3xy^2 \tag{33}$$

A Dirichlet problem and a Neumann problem are solved for which the essential boundary condition and the natural boundary condition are imposed on all edges respectively, and a mixed problem for which the essential boundary condition is imposed on top and bottom edges and the natural boundary condition is prescribed on left and right edges of the domain.

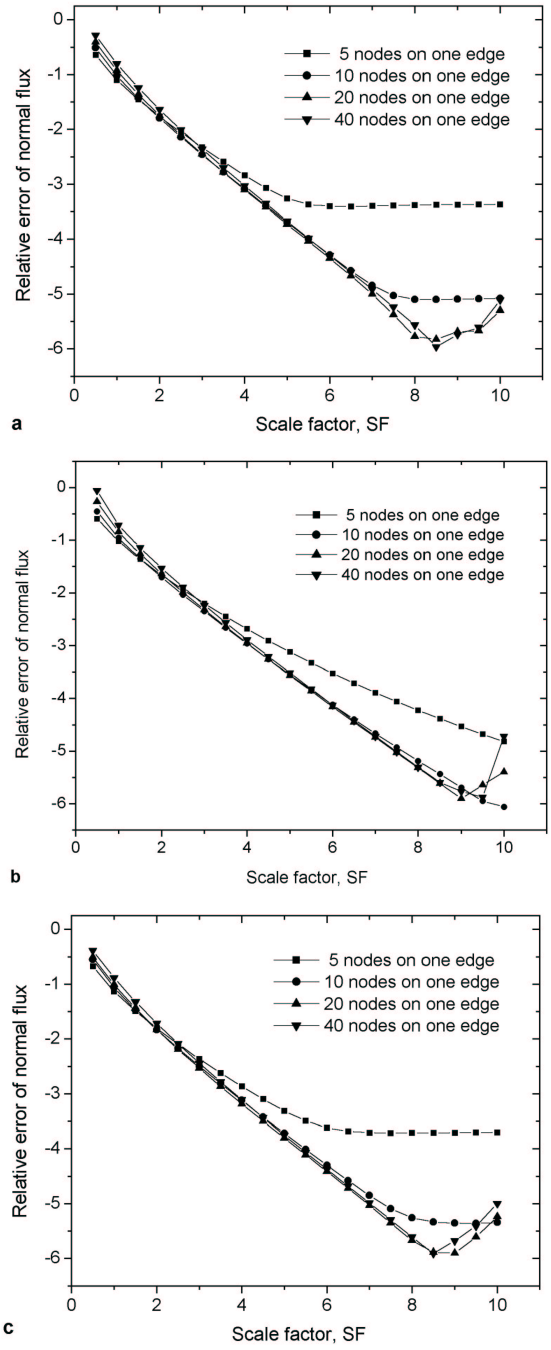

Figure 4 : Relative errors of normal flux on the edge (from (0,0) to (2,0)): **a** for Dirichlet problem, **b** for Neumann problem, **c** for mixed problem

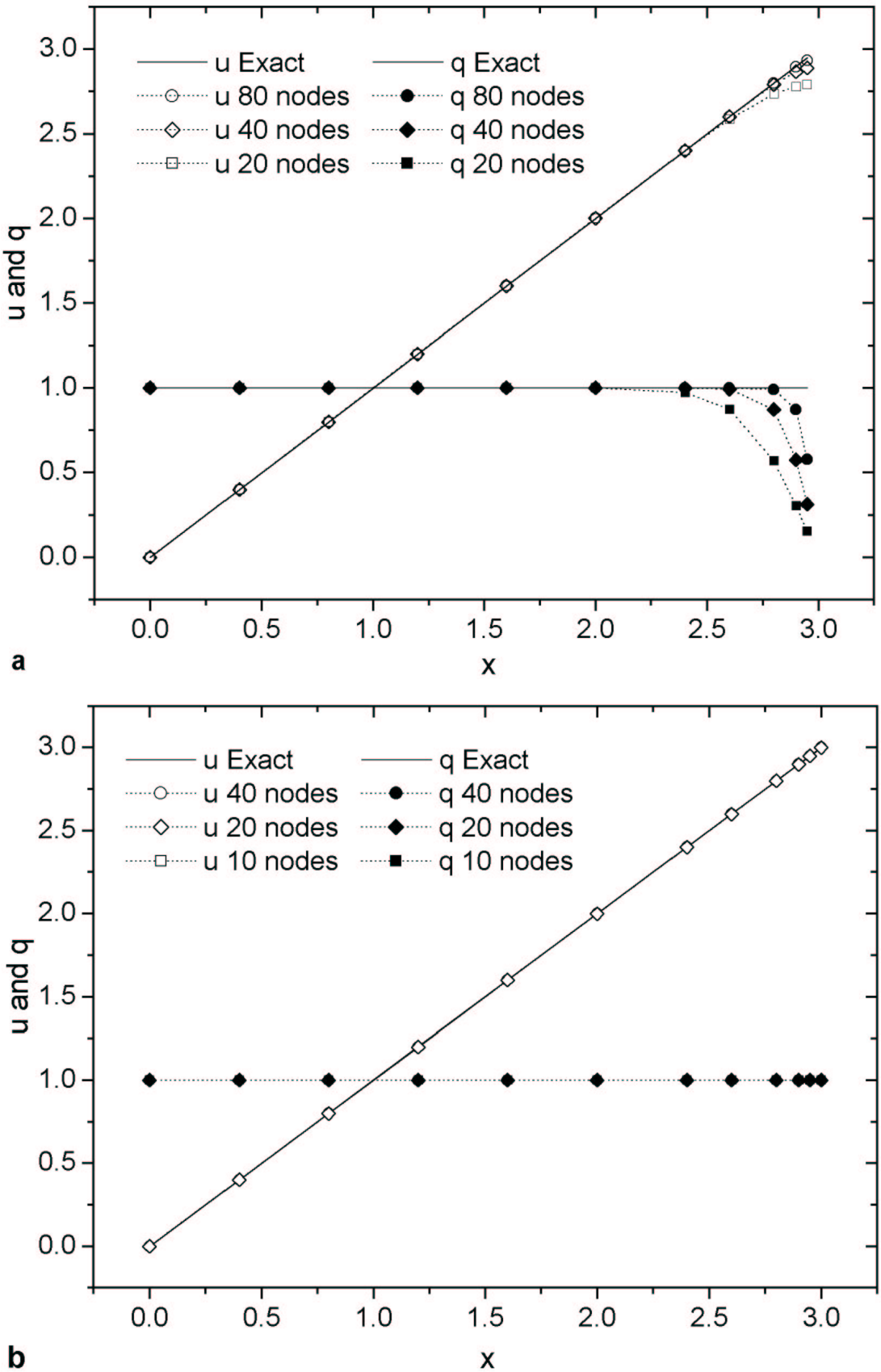

Figure 3 : u and q along a radius (from (0,0) to (3,0)): **a** from Hybrid BNM. **b** from RHBNM

The effect of the selection of the scale factor *SF* has been studied on four different regular nodes arrangements: (a) 5 nodes on each edge; (b) 10 nodes on each edge; (c) 20 nodes on each edge; (d) 40 nodes on each edge, with *SF* varying from 0.5 to 10. Fig. 4 shows the relative errors (equation (31)) of normal flux on the edge (from (0,0) to (2,0), 13 uniformly distributed sample points) with different meshes. It is noted that the results for all meshes are accurate enough when $SF \geq 3.0$. However, as *SF* grows beyond 8.5, results become unstable for the meshes (b), (c) and (d). This implies that the equations (27) and (28) are approaching nearly ill-posed. Actually, further computations of this example show that the biggest values of *SF* that ensure the RHBNM non-degenerate are 11.0, 11.5, 15.5 and 32.5 for the meshes (a), (b), (c) and (d), respectively, and these values are independent of boundary conditions while dependent on the domain geometry and meshing.

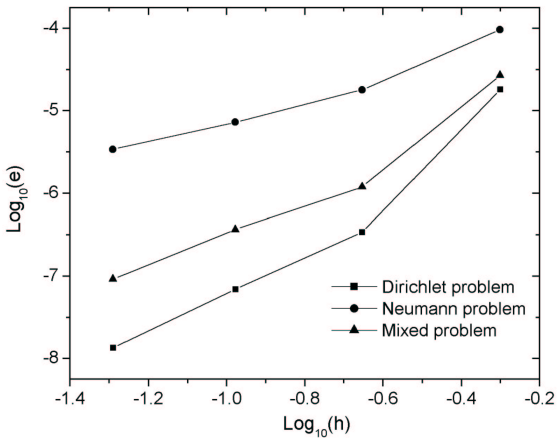

Figure 5 : Relative errors and convergence rates for Dirichlet, Neumann and mixed problems.

The convergence of the method has also been studied on the four nodes arrangements with $SF = 5.0$. The results of relative errors (equation (31)) and convergence of potential on the diagonal (from (0,0) to (2,2), 19 uniformly distributed sample points) are shown in Fig. 5, and numerical results of normal flux on the edge (from (0,0) to (2,0)) from the RHBNM when 5 nodes are used on each edge, together with the exact solution are shown in Fig. 6. It can be seen that the present RHBNM has high rates of convergence and the numerical results almost reproduce the exact solution exactly.

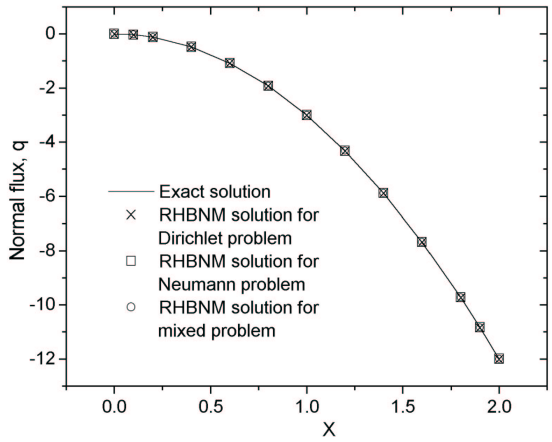

Figure 6 : $q(x)$ at $y = 0$ for Dirichlet, Neumann and mixed problems (5 nodes on each edge are used)

4.3 Potential flow

The third example, which has been described in Atluri et al. (1998), Zhu et al. (1998) and Zhu (1999), is the problem of a potential flow around a cylinder of radius 1 in an infinite domain, *u* represents the stream function. Due to the symmetry of the problem, only a part, $0 \leq x \leq 4$ and $0 \leq y \leq 2$, of the upper left quadrant of the field is modeled as shown in Fig. 2. The exact solution for this problem is given by

$$u = y\left[1 - \frac{a^2}{y^2 + (x-L)^2}\right] \tag{34}$$

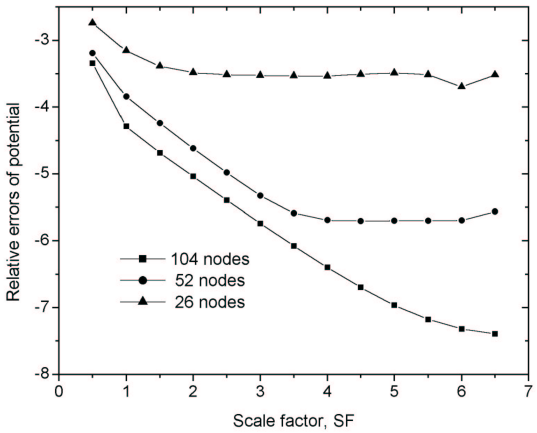

Figure 8 : Relative errors and convergence rates for the potential flow problem

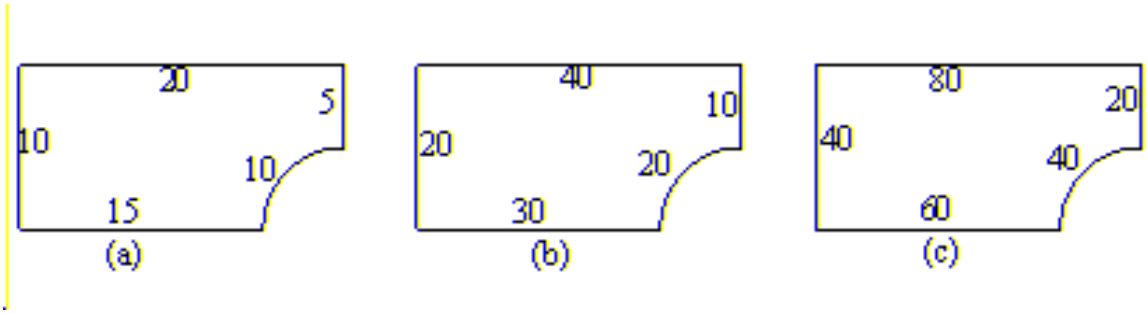

Figure 7 : Flow around a cylinder; nodal arrangement: (a) 26 nodes; (b) 52 nodes; (c) 104 nodes

The prescribed u and q along all boundaries are shown in Fig. 2. The essential boundary condition on the left and top edges is imposed according to the exact solution. The nodal arrangements are shown in Fig. 7.

The effect of SF has also been studied in this problem. In this case, the value for SF varies from 0.5 to 6.5 and the results of relative errors (equation (31)) of potential on the diagonal (from (0,0) to (4,2), 19 uniformly distributed sample points) are shown in Fig. 8. It is appealing that the results are most accurate for all SF values. The RHBNM, if anything, is somewhat flexible.

In this example, the biggest values of SF that ensure the RHBNM non-degenerate for the meshes (a), (b) and (c) are 13.5, 6.5 and 8.0, respectively. Unfortunately, it seems that no simple rule exists between the biggest SF value and the nodes arrangement. Further work is required in this area.

High rates of convergence can also be observed in Fig. 8. Numerical results along the arc (from (3,0) to (4,1)) from the RHBNM with $SF = 5.0$, together with the exact solution, are shown in Fig. 9. The numerical results agree excellently with the exact solutions again.

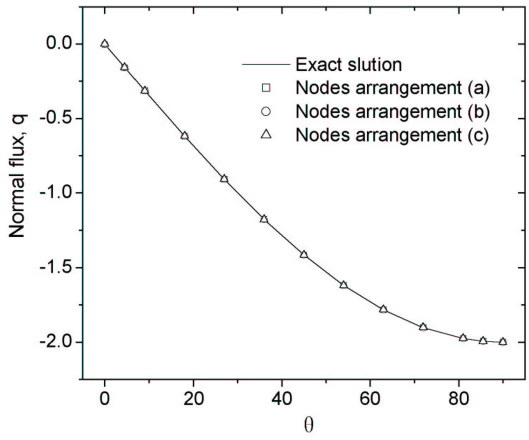

Figure 9 : $q(\theta)$ along the arc with different node arrangements

5 Conclusions and discussion

A new type of regular hybrid boundary node method has been presented in this paper. It is based on a hybrid model that involves three types of independent variables, i.e. potentials and normal fluxes on the boundary and potentials inside the domain, and coupled with the MLS interpolation scheme over the boundary variables. Compared with the MLBIE and MLPG, the new approach has the well-known dimensionality of the BEM, e.g. for a 3-D object, only randomly distributed nodal points are required to be constructed on the 2-D bounding surface of a body; compared with the conventional BEM, it is a meshless method, only requires a nodal data structure on the bounding surface of the domain to be solved; compared with the BNM, it is a truly meshless method, absolutely no cells are needed either for interpolation purposes or for integration purposes.

Numerical examples have shown the accuracy and convergence of the results. The solution is most accurate for the potentials and fluxes on the boundary and in the domain. High rates of convergence have been achieved. And high accuracy can be obtained with a small number of nodes.

In contrast with the conventional BEM, reduced to the solution of the singular-integral equations of the second kind, the RHBNM leads to regular-integral equation of the first kind. No singularities are involved, the evaluation of variables at internal points does not demand any integration as in the conventional BEM or the BNM, and the serious "boundary layer effect" in the Hybrid BNM is largely circumvented.

However, the outside assignment of the source points of the fundamental solutions causes some new problems, for example, how to choose the value of the scale factor, SF? Where to put the source points when a concave boundary, a crack for example, is considered? The answer for the first question is only an empirical recommendation by now, just as the other constant parameters in equations (11) and (21). For the second question, the multi-domain approach is recommended. Actually, like the BEM, if the RHBNM is to be developed to solve large scale and complicated structures in practical engineering, it must be coupled with the Multi-domain and Multi-pole method (Popov et al., 2001). And these are planned investigations for the future.

Though some drawbacks exist, e.g. many constant parameters have to be determined by experience, the advantages of the RHBNM, such as meshless nature, very high accuracy, high convergence rates and no singularities etc., are so attractive that this method is certainly worthy of attention.

References

Atluri SN, Kim HG, Cho JY (1999) A critical assessment of the truly Meshless Local Petrov-Galerkin (MLPG), and Local Boundary Integral Equation (LBIE) methods. Computational Mechanics. 24:348-372.

Atluri SN, Zhu T (1998) A new meshless local Petrov-Galerkin approach in computational mechanics. Computational Mechanics. 22:117-127.

Belytchko T, Krongauz Y, Organ D (1996) Fleming M, Krysl P. Meshless methods: an overview and recent developments. Computer Methods in Applied Mechanics and Engineering. 139:3-47.

Belytchko T, Lu YY, Gu L (1994) Element free Galerkin methods. International Journal for Numerical Methods in Engineering. 37:229-256.

DeFigueredo TGB, Brebbia CA (1989) A new hybrid displacement variational formulation of BEM for elastostatics. Brebbia CA and Conner JJ (eds.), Advances in Boundary Elements, CMP. 1:47-57.

Dumount NA (1987) The hybrid boundary element method. Proceedings 9th International Conference On BEM. Stuttgart, Computational Mechanics Publications. Southampton and Springer Verlag, Berlin.

Kim HG, Atluri SN (2000) Arbitrary Placement of Secondary Nodes and Error Control in the Meshless Local Petrov-Galerkin (MLPG) Method. Computer Modeling in Engineering & Sciences. 1(3):11-32.

Lancaster P, Salkauskas K (1981) Surfaces generated by moving least squares methods. Mathematics in Computation. 37:141-158.

Lin H, Atluri SN (2000) Meshless Local Petrov-Galerkin (MLPG) Method for Convection-Diffusion Problems. Computer Modeling in Engineering & Sciences. l.1(2): 45-60.

Lucy LB (1977) A numerical approach to the testing of the fission hypothesis. The Astronomy Journal. 8:1013-1024.

Mukherjee YX, Mukherjee S (1997) The boundary node method for potential problems. International Journal for Numerical Methods in Engineering. 40:797-815.

Nayroles B, Touzot G, Villon P (1992) Generalizing the finite element method: Diffuse approximation and diffuse element. Computational Mechanics. 10:307-318.

Popov V, Power H (2001) An O(N) Taylor series multipole boundary element method for three-dimensional elasticity problems. Engineering Analysis with Boundary Elements.25:7-18.

Schnack E (1987) A hybrid BEM model. International Journal for Numerical Methods in Engineering 24:1015-1025.

Zhang JM, Yao ZH, Li H. A hybrid boundary node method. International Journal for Numerical Methods in Engineering, accepted.

Zhu T (1999) A new meshless regular local boundary integral equation (MRLBIE) approach. International Journal for Numerical Methods in Engineering. 46:1237-1252.

Zhu T, Zhang J, Atluri SN (1998) A local boundary integral equation (LBIE) method in computation mechanics, and a meshless discretization approach. Computational Mechanics. 21:223-235.